Supporting Information

Al-Sc Dual Doped LiGe$_2$(PO$_4$)$_3$ - a NASICON-Type Solid Electrolyte with Improved Ionic Conductivity

Yosef Nikodimos[a, c], Meng-Che Tsai[b], Ljalem Hadush Abrha[a], Haile Hisho Weldeyohannis[a], Shuo-Feng Chiu[a], Hailemariam Kassa Bezabh[a], Kassie Nigus Shitaw [a], Fekadu Wubatu Fenta[a], She-Huang Wu[b, c], Wei-Nien Su[b], Chun-Chen Yang[c, d], Bing-Joe Hwang[a, e, f]

a. Nano-electrochemistry Laboratory, Department of Chemical Engineering, National Taiwan University of Science and Technology, Taipei city 106, Taiwan

b. Nano-electrochemistry Laboratory, Graduate Institute of Applied Science and Technology, National Taiwan University of Science and Technology, Taipei city 106, Taiwan

c. Battery Research Center of Green Energy, Ming Chi University of Technology, New Taipei City 24301, Taiwan

d. Department of Chemical Engineering, Ming Chi University of Technology, New Taipei City 24301, Taiwan

e. National Synchrotron Radiation Research Center (NSRRC), Hsinchu 30076, Taiwan

f. Sustainable Energy Development Center, National Taiwan University of Science and Technology, Taipei city 106, Taiwan

Electronic conductivity measurement: The electronic conductivity of the solid electrolyte pellet was measured by a standard four-point probe technique (KeithLink Technology, Taiwan). An LASGP1 pellet (13 mm diameter and 0.5 mm thickness), pressed using a steel die in a hydraulic press under a pressure of 2500 MPa for 5 minutes, was used for the electronic conductivity measurement. The four-point probe measurement was performed at three different sites on two LASGP1 pellets to get reliable average electronic conductivity.

Defect formation energy: The defect formation energy was calculated for different sites to find the most stable site. The defect formation energy was calculated as follow[1]:

$$E_{defect} = E_{pure} - E_{doped} + \sum_{N}^{i} \Delta n_i \mu_i \qquad (1)$$

where E_{doped} and E_{pure} are the total energy of the supercell with and without the dopants, respectively; Δn_i is the number of atoms of element i added to (or removed from) the supercell to create charge balance the supercell; and μ_i is the chemical potential of element i. This is summed for all elements N, which are added or removed during the doping reaction.

Li ion hopping analysis: The Li migration was investigated from the AIMD simulations by timing of hopping events. A hopping event was identified for each Li^+ then counted at the time when the ion changes its site. A 2 ps average time for the Li^+ spatial position is used to prevent from counting a local high-frequency vibration. Furthermore, a statistical analysis for the time of all Li ion hopping events in AIMD simulations was performed. Li ions hopping occurring within 1 ps were grouped as one individual concerted migration event, and the number of Li ions, *n*, is determined for each migration event.

Table S1: Finding the most stable sites of Li in the LASGP1 sample

M_2 Site	E_{defect} (eV)	Site	E_{defect} (eV)
1, 2, 3	2.350	2, 3, 4	1.980
1, 2, 4	1.998	**2, 3, 5**	**1.008**
1, 2, 5	1.927	2, 3, 6	1.924
1, 2, 6	1.929	2, 4, 5	1.947
1, 3, 4	1.985	2, 4, 6	1.958
1, 3, 5	2.031	2, 5, 6	1.938
1, 3, 6	1.994	3, 4, 5	2.081
1, 4, 5	1.933	3, 4, 6	2.166
1, 4, 6	1.929	4, 5, 6	1.947
1,5, 6	1.927		

Table S2: Finding the most stable sites of Al and Sc in the LASGP1 sample

Finding the most stable site of Al				Finding the most stable site of Sc	
Substituted Ge site	E_{defect} (eV)	Substituted Ge site	E_{defect} (eV)	Substituted Ge site	E_{defect} (eV)
1st, 2nd	2.360	4th, 6th	2.362	1st	2.359
1st, 3rd	2.364	4th, 7th	2.357	3rd	2.362
1st, 4th	2.358	4th, 8th	2.363	4th	2.360
1st, 5th	2.359	4th, 9th	2.361	5th	2.359
1st, 6th	2.365	4th, 10th	2.365	6th	2.365
1st, 7th	2.365	4th, 11th	2.358	7th	2.361
1st, 8th	2.361	5th, 6th	2.364	8th	2.358
1st, 9th	2.355	5th, 7th	2.365	9th	2.364
1st, 10th	2.359	5th, 8th	2.363	10th	2.359
1st, 11th	2.357	5th, 9th	2.361	12th	2.363
2nd, 3rd	2.364	5th, 10th	2.355		
2nd, 4th	2.356	5th, 11th	2.360		
2nd, 5th	2.364	6th, 7th	2.361		
2nd, 6th	2.355	6th, 8th	2.359		
2nd, 7th	2.358	6th, 9th	2.365		
2nd, 8th	2.356	6th, 10th	2.360		
2nd, 9th	2.355	6th, 11th	2.365		
2nd, 10th	2.358	7th, 8th	2.360		
2nd, 11th	2.363	7th, 9th	2.361		
3rd, 4th	2.359	7th, 10th	2.358		
3rd, 5th	2.364	7th, 11th	2.361		
3rd, 6th	2.357	8th, 9th	2.358		
3rd, 7th	2.363	8th, 10th	2.359		
3rd, 8th	2.362	8th, 11th	2.359		
3rd, 9th	2.356	9th, 10th	2.356		
3rd, 10th	2.363	9th, 11th	2.361		
3rd, 11th	2.361	10th, 11th	2.363		
4th, 5th	2.362				

Table S3: Experimental lattice parameter decrement expressed in percentage relative to its respective DFT value

	Change of lattice parameters relative to DFT values (%)		
Sample	a	c	V
LAGP	1.77%	2.00%	1.15%
LASGP1	0.99%	1.15%	0.74%
LASGP2	2.15%	2.30%	1.48%
LSGP	2.61%	3.70%	2.09%

Table S4: Intragrain elements analysis using EDX technique for different $Li_{1.5}Al_xSc_yGe_{1.5}(PO_4)_3$ electrolyte samples corresponding to Fig S4 (a-d).

Element	EDX analysis (weight%)			
	LAGP	LASGP1	LASGP2	LSGP
Al	3.324	2.170	1.118	-
Sc	-	1.863	3.616	4.496
Ge	26.494	26.556	25.850	26.044
P	22.896	22.645	22.646	22.661
O	47.286	46.766	46.770	46.799
Li	-	-	-	-
Overall formula	$Li_{1.5}Al_{0.5}Ge_{1.48}(PO_4)_3$	$Li_{1.5}Al_{0.33}Sc_{0.17}Ge_{1.5}(PO_4)_3$	$Li_{1.5}Al_{0.17}Sc_{0.33}Ge_{1.46}(PO_4)_3$	$Li_{1.5}Sc_{0.41}Ge_{1.47}(P_{0.97}O_4)_3$

Table S5: Elements analysis on grain boundaries using EDX technique for different $Li_{1.5}Al_xSc_yGe_{1.5}(PO_4)_3$ electrolyte samples corresponding to Fig S4 (e-g).

Element	EDX analysis (weight%)		
	LAGP	LASGP2	LSGP
Al	0.101	0.010	-
Sc	-	0.109	23.393
Ge	67.604	67.54	18.897
P	1.090	0.941	16.113
O	31.205	31.4	41.597
Li	-	-	-
Result	GeO_2	GeO_2	$GeO_2 + 2ScPO_4$

Table S6: Diffusivity and activation energy (overall and in different directions) of the $Li_{1+x+y}Al_xSc_yGe_{2-x-y}(PO_4)_3$ electrolytes from AIMD simulations at 25 ^{o}C

Sample	Z-direction		XY plane		Total	
	$D \times 10^{-6}$ (cm^2/s)	E_a (eV)	$D \times 10^{-6}$ (cm^2/s)	E_a (eV)	$D \times 10^{-6}$ (cm^2/s)	E_a (eV)
LAGP	1.140 ± 0.006	0.101	0.111 ± 0.003	0.4	0.821 ± 0.003	0.286
LASGP1	1.850 ± 0.003	0.0973	1.040 ± 0.001	0.316	1.550 ± 0.002	0.279
LASGP2	0.341 ± 0.004	0.349	0.0125 ± 0.003	0.502	0.119 ± 0.003	0.420
LSGP	0.219 ± 0.004	0.371	0.0014 ± 0.004	0.557	0.0193 ± 0.004	0.461

Table S7: Estimated channel sizes for each $Li_{1+x+y}Al_xSc_yGe_{2-x-y}(PO_4)_3$ sample after optimization

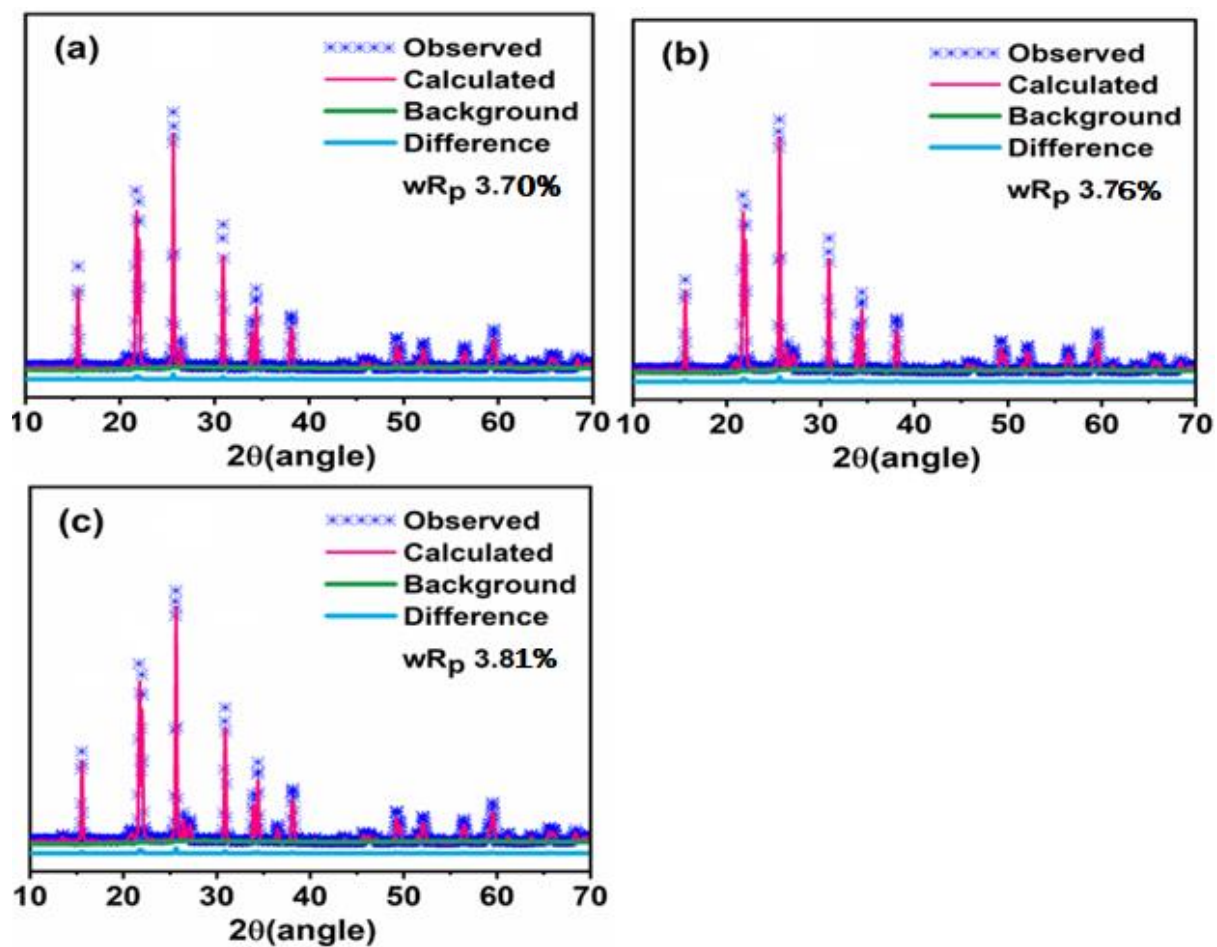| Sample	Average r(Å)	Volume of LiO_6 (Å^3)
LAGP	2.229	34.774
LASGP1	2.258	35.349
LASGP2	2.363	36.831
LSGP	2.415	38.226

Table S8: Li-Al and Li-Sc coordination in $Li_{1+x+y}Al_xSc_yGe_{2-x-y}(PO_4)_3$ electrolyte samples

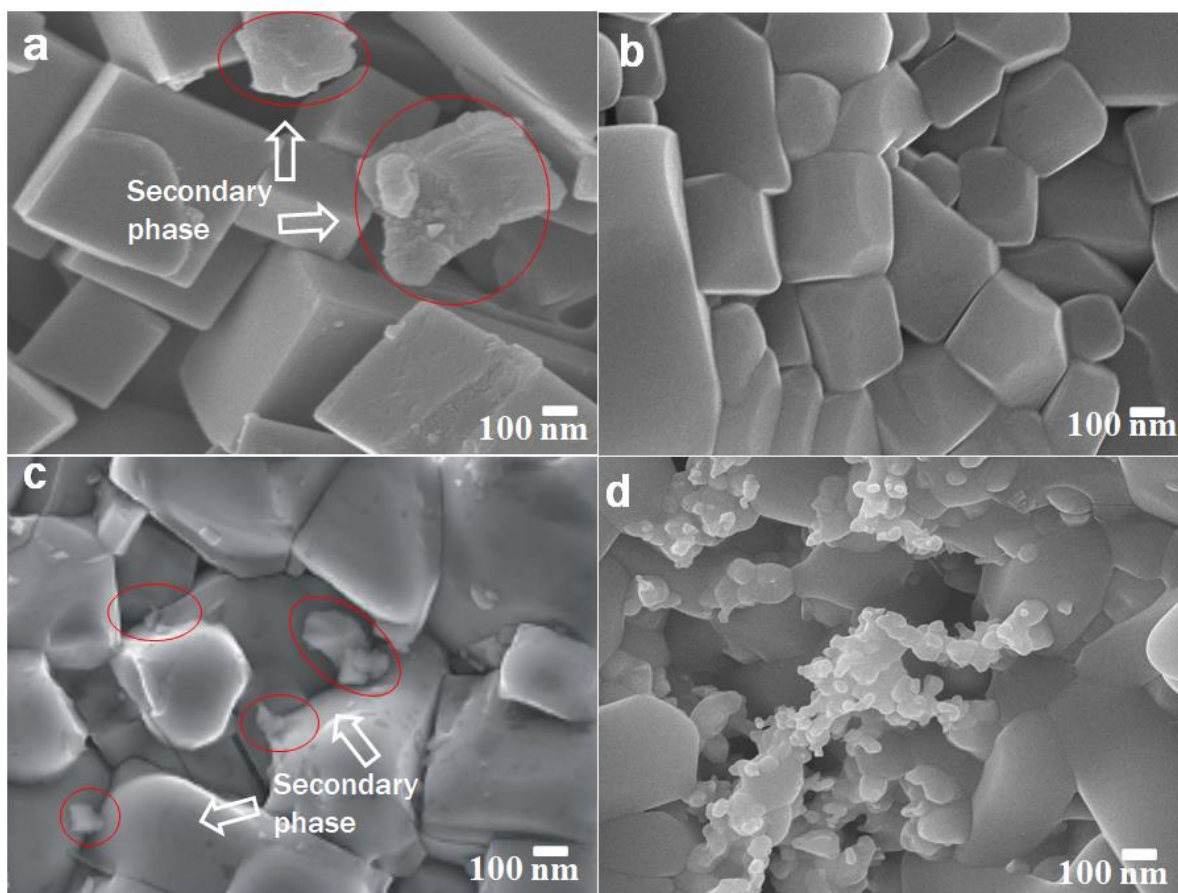| $Li_{1+x+y}Al_xSc_yGe_{2-x-y}(PO_4)_3$	Li concentration near to:	
	Al	Sc
LAGP	2.45	-
LASGP1	1.29	0.88
LASGP2	0.67	2.86
LSGP	-	4.64
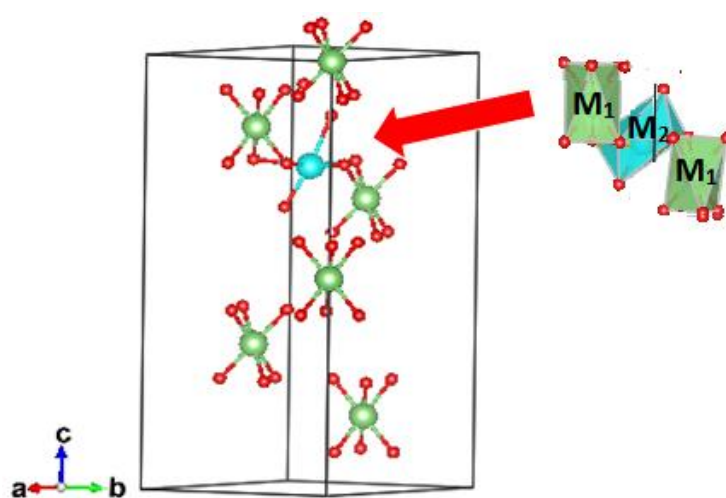
Fig S1: M_1 and M_2 sites of Li atoms in the crystal structure of $LiGe_2(PO_4)_3$

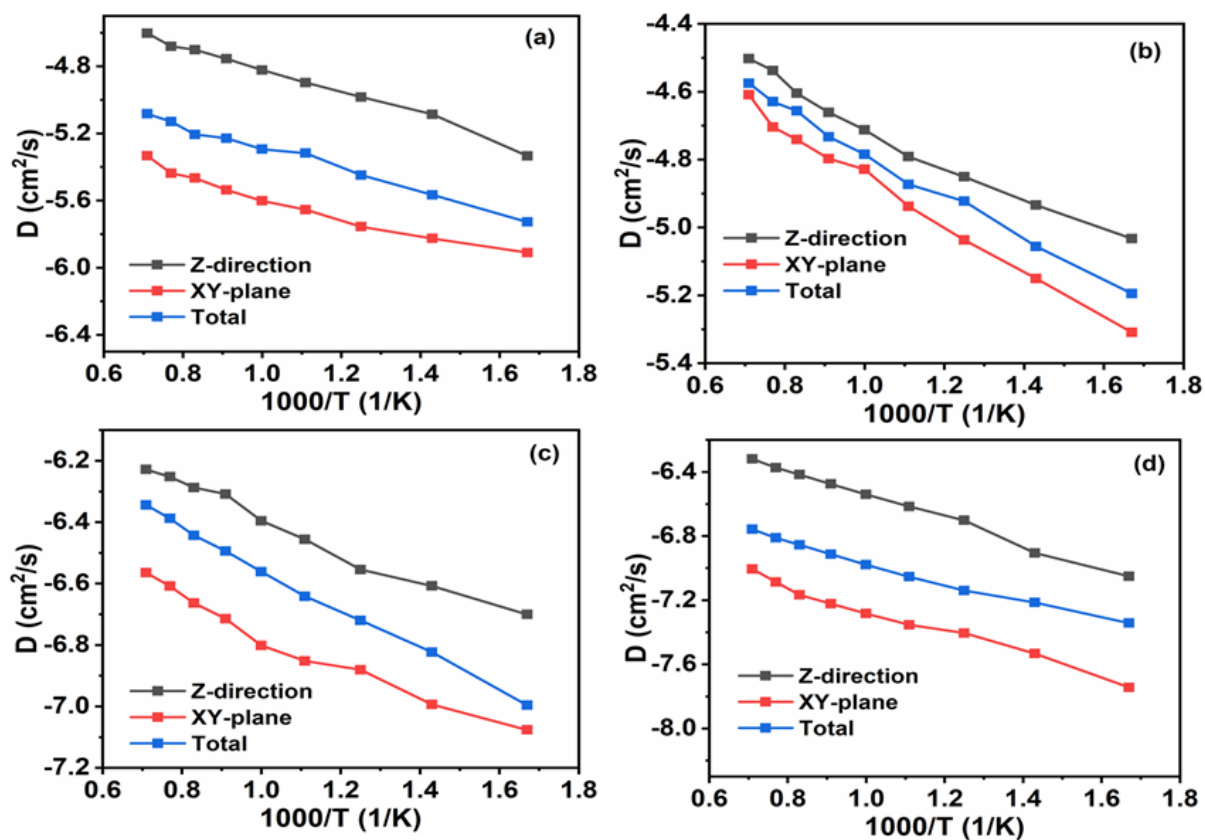**Fig S2:** Rietveld refined XRD patterns of (a) LAGP, (b) LASGP2 and (c) LSGP

Fig S3: FE-SEM images of $Li_{1+x+y}Al_xSc_yGe_{2-x-y}(PO_4)_3$ electrolyte samples (a) LAGP (b) LASGP1 (c) LASGP2 and (d) LSGP
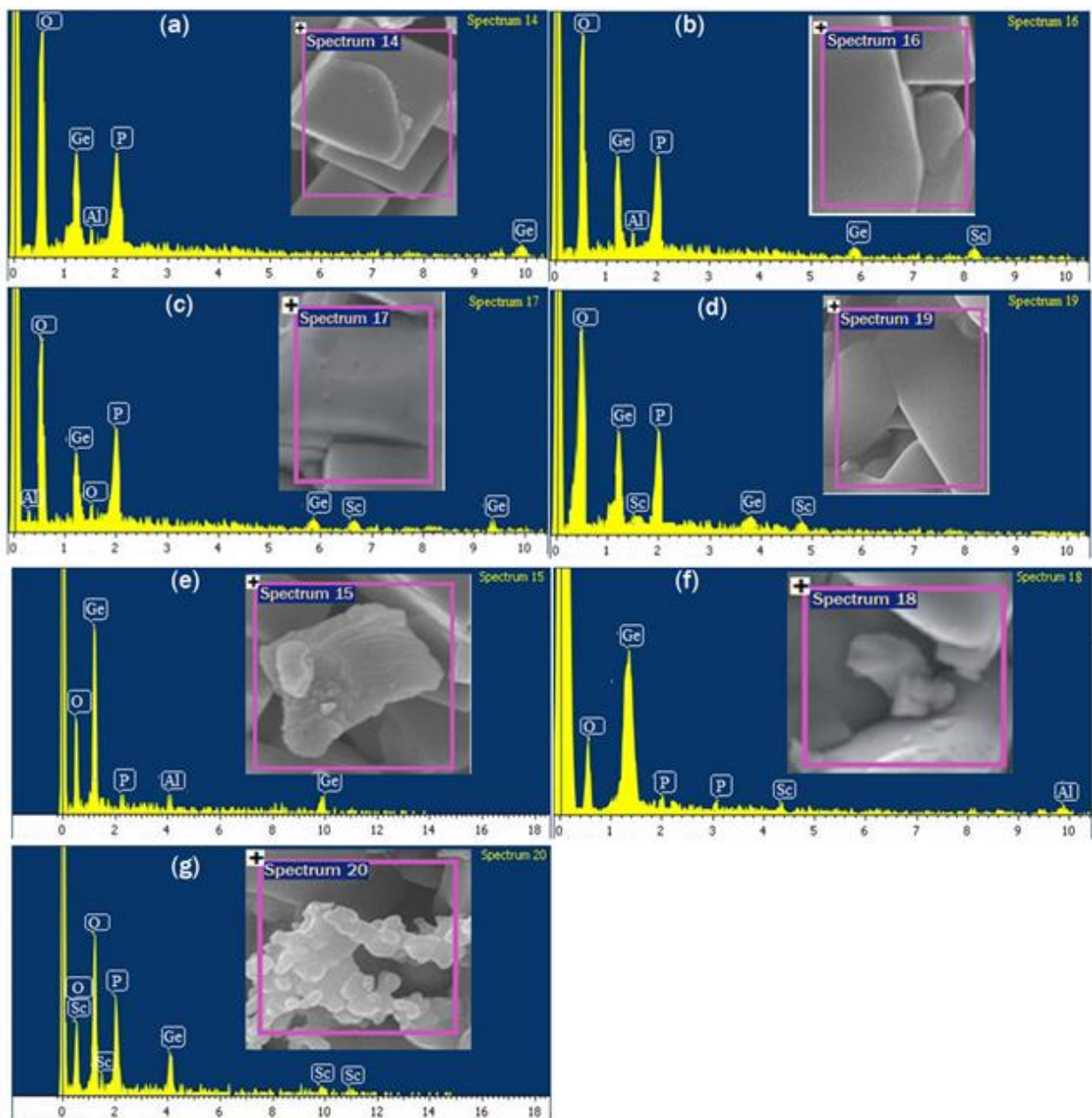
Fig S4: EDX element distribution of $Li_{1+x+y}Al_xSc_yGe_{2-x-y}(PO_4)_3$ electrolyte samples on intragrain zone (a) LAGP, (b) LASGP1, (c) LASGP2, (d) LSGP and grain boundary zone (e) LAGP, (f) LASGP2 (g) LSGP
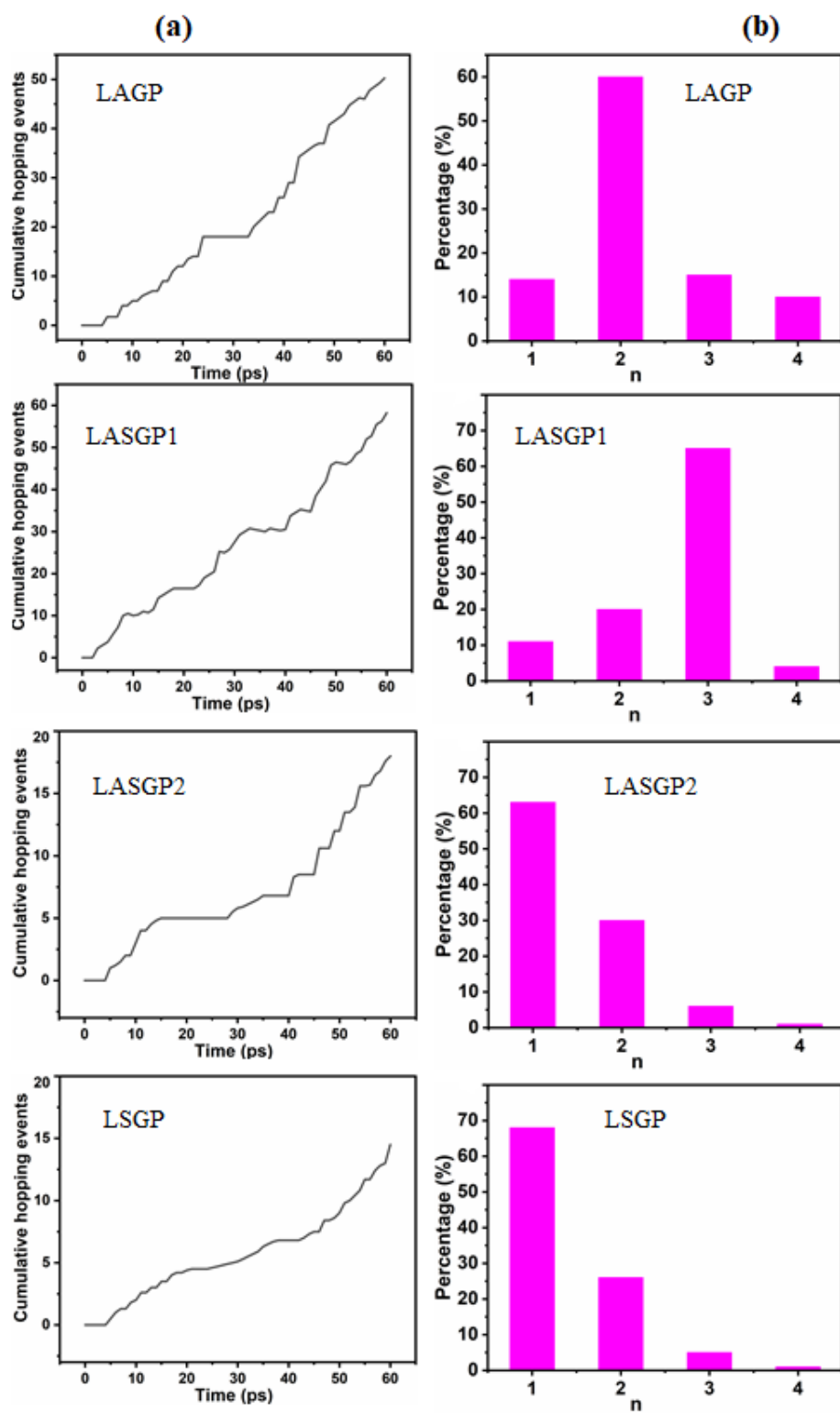
Fig S5: Arrhenius plot of the diffusion coefficient in the Z direction, in the XY plane and overall: (a) LAGP (b) LASGP1 (c) LASGP2 (d) LSGP
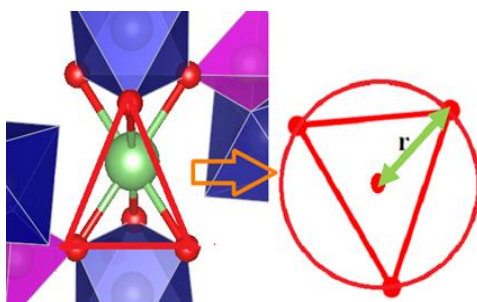

Fig S6. Schematic for the channel size determination for all d-LGP electrolytes.
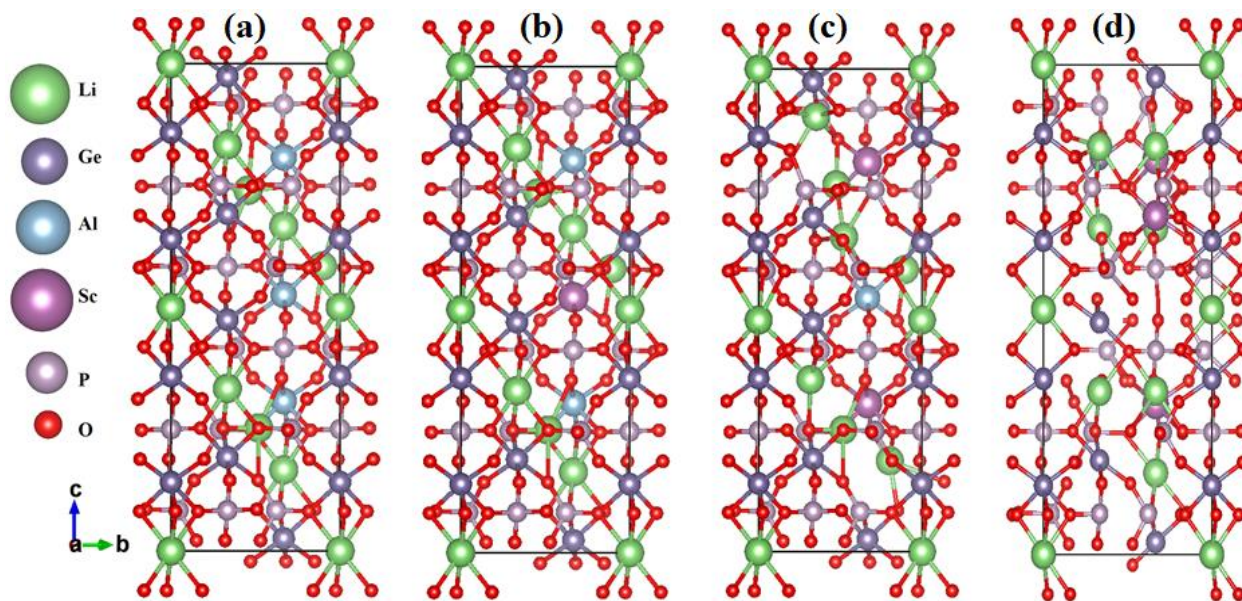
Fig S7: Crystal structures after relaxation: (a) LAGP, (b) LASGP1, (c) LASGP2 and (d) LSGP

Fig S8: Li ions hopping event analysis in $Li_{1.5}Al_xSc_yGe_{1.5}(PO_4)_3$ electrolyte samples: (a) Plot of cumulative hopping events versus time and (b) histograms for the number of Li ions, *n*, hopping from AIMD simulations at 900 K
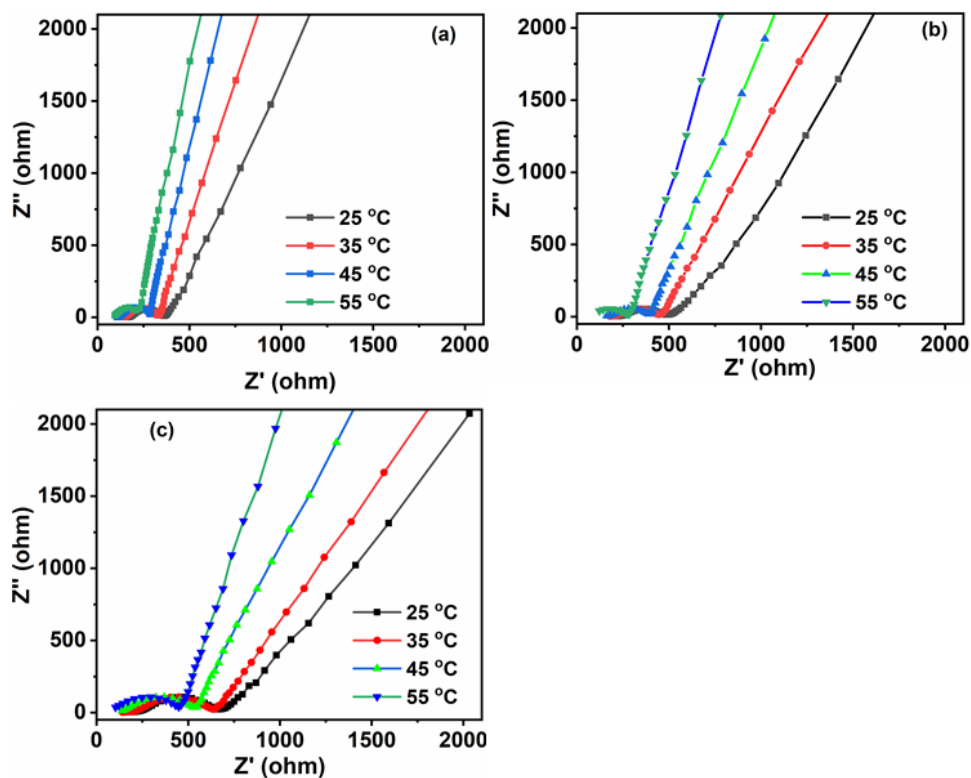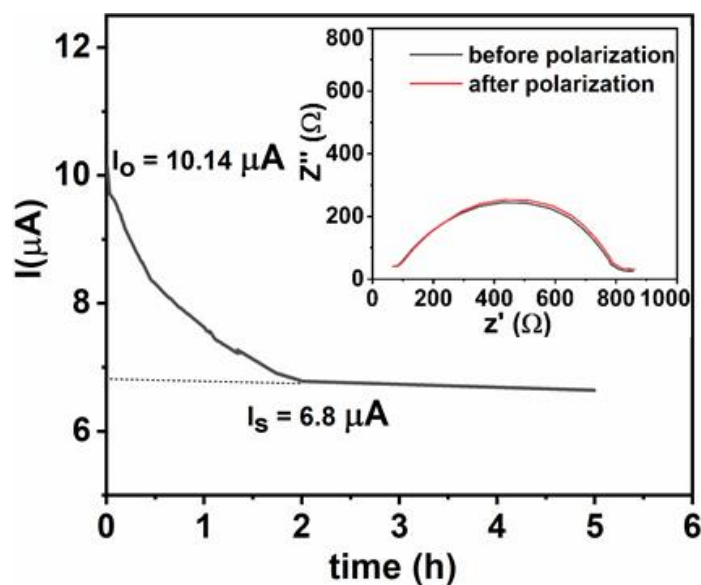
Fig S9: Nyquist plots measured in the frequency range of $10^{-2} - 10^6$ Hz and temperature range of 25–55 °C (a) LAGP, (b) LASGP2, (c) LSGP
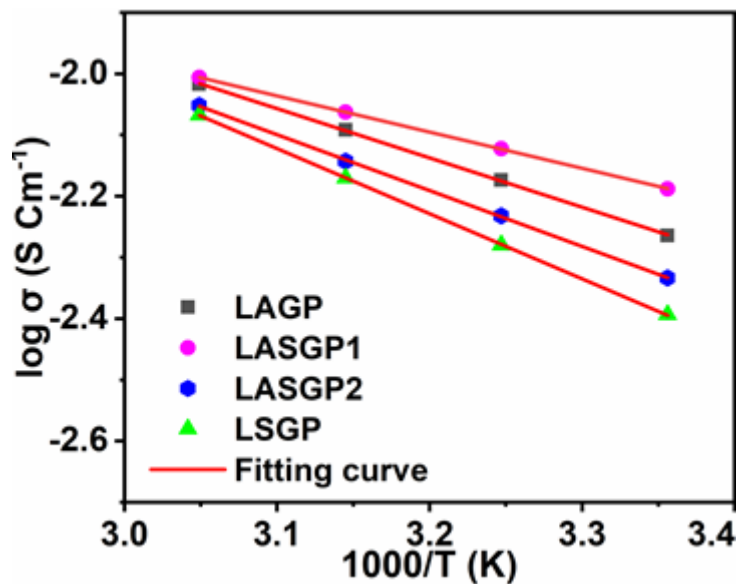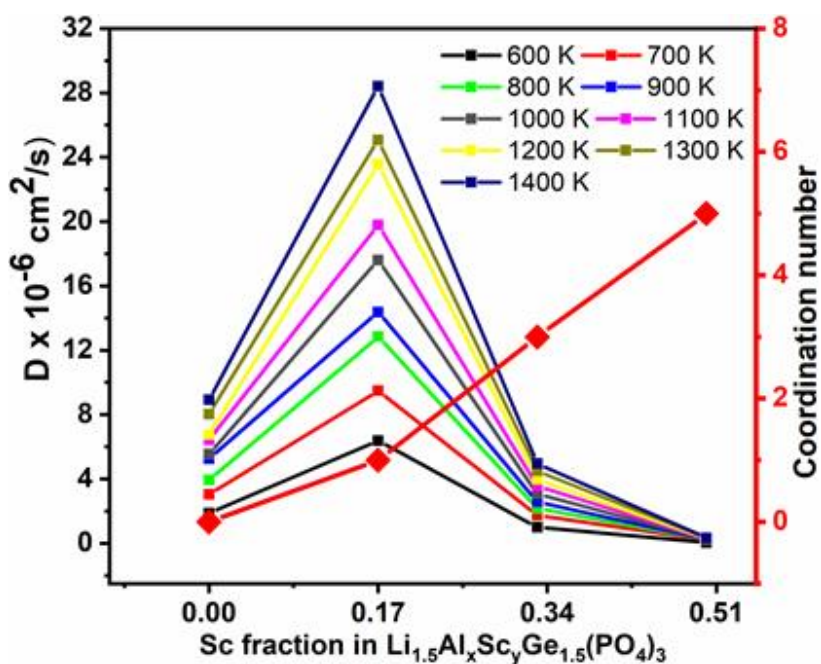

Fig S10: Ionic conductivity variation of $Li_{1+x+y}Al_xSc_yGe_{2-x-y}(PO_4)_3$ electrolyte samples with temperature, as well as their fitting curves

Fig S11: Current-time curve obtained from chronoamperometry at a DC polarization of 0.01V for Li/LASGP1/Li symmetric cell. inset: Nyquist profiles of the cell before and after polarization

Fig S12: Li$^+$ diffusivity and Li-Sc coordination in Li$_{1+x+y}$Al$_x$Sc$_y$Ge$_{2-x-y}$(PO$_4$)$_3$ electrolyte samples with respect to Sc amount.

Reference

1.   L. J. Miara, W. D. Richards, Y. E. Wang and G. Ceder, *Chem. Mater.*, 2015, **27**, 4040-4047.